Bachelor Degree Project

Feigenbaum Scaling

Author: Janek Sendrowski
Supervisor: Hans Frisk
Semester: HT 2019/VT 2020
Subject: Mathematics

Abstract

In this thesis I hope to provide a clear and concise introduction to Feigenbaum scaling accessible to undergraduate students. This is accompanied by a description of how to obtain numerical results by various means. A more intricate approach drawing from renormalization theory as well as a short consideration of some of the topological properties will also be presented. I was furthermore trying to put great emphasis on diagrams throughout the text to make the contents more comprehensible and intuitive.

Contents

List of Figures

List of Tables

1 Introduction

In 1978, M. J. Feigenbaum published a paper describing a behavior universal to certain families of non-linear one-hump maps of which the *logistic map* is a popular example [1]. This *universality* initially caused a lot of excitement in the scientific community with many people being puzzled as to how e.g. two maps as different as $\mu x(1-x)$ and $\mu x^2 \sin(\pi x)$ could give rise to the same constants when iterated. Feigenbaum himself managed to provide a deeper insight partly by making use of *renormalization theory* borrowed from statistical mechanics [3].

The non-linear nature of these maps when iterated can result in chaotic behavior as small perturbations in the initial value are repeatedly amplified and mapped onto the same bounded interval. The logistic map was in fact suggested as a random number generator in the early days of computers [4]. However, one of the most striking properties is the *self-similar* nature of these maps thus making them susceptible to renormalization procedures. Their otherwise rather straightforward definition makes them easily applicable to real-world models and shows that very complex behavior can arise under simple circumstances. One notable although perhaps oversimplified application is that of the logistic map to population dynamics where a population experiences exponential growth for sizes significantly lower than the carrying capacity with starvation dampening or reversing the growth otherwise [7]. The Feigenbaum constant, one of the universal constants, could also be verified experimentally in real-world phenomena like fluid dynamics, acoustics, optics and electronics [4].

The purpose of this work is to provide the undergraduate reader with a concise introduction to Feigenbaum scaling as well as touching on more advanced disciplines such as functional analysis and topology within the framework of the thesis. The deepened insight brought forward by these disciplines hopefully vindicates their use. After this introduction will follow the theory part introducing some necessary concepts of dynamical systems such as fixed points and orbits (section 2). This is followed by section 3 which explains the basics of Feigenbaum scaling. It begins with the definition of the map in questions, then treats the final-state diagram and finally introduces the universal constants based on the regime of the successive period-doubling bifurcations together with the class of maps for which this universality is valid. This section makes heavy use of the concepts introduced in the theory part. Next, section 4 establishes the use of renormalization theory which is necessary to understand section 6.2 in the computational part. This section

draws on functional analysis as we are now considering the stability of the period-doubling operator F in function space. The following section (5) is mainly concerned with the topological properties at and beyond the Feigenbaum point. A short description about the characteristics of chaos will also be given. In sections 4 & 5, some new concepts are introduced at the point when they are needed. Subsequently, there will be a computational part (6) which begins with the calculation of the Feigenbaum constant via the direct method (section 6.1). In the following two subsections, the computation of the spectrum of the linearized period-doubling operator and generalized Feigenvalues will be described (sections 6.2 & 6.3). The material from section 3 is essential in order to understand sections 6.1 & 6.3. The thesis is then coming to an end with a short conclusion (7). The Mathematica code for the generation of all of the figures as well as the implementation of the computational part (6) can be found online [14].

2 Theory

2.1 Sequence of iterates

We now introduce some terminology that will be necessary to understand the ensuing discussion. By the *sequence of iterates* or simply the *iterates* of a map f we mean the sequence

$$\{x_n\}_{n=0}^{\infty} = \{f^n(x_0)\}_{n=0}^{\infty}, \quad x_0 \in I,$$

where

$$f^n(x) = \underbrace{f \circ f \circ ... \circ f}_{\text{n times}}(x)$$

denotes the n-fold composition of f which we call its nth *iterate* and where $f^0(x_0) := x_0$. The interval I denotes here the domain of f.

2.2 Fixed points

The point $\hat{x}$ is called a *fixed point* if $f(\hat{x}) = \hat{x}$ is satisfied. Let the sequence of iterates $\{f^n(x_0)\}_0^{\infty}$ be given. If it is convergent with limit $\hat{x}$, then $\hat{x}$ is a fixed point of f as

$$f(\hat{x}) = f\left(\lim_{n\to\infty} x_n\right) = \lim_{n\to\infty} f(x_n) = \lim_{n\to\infty} x_{n+1} = \hat{x},$$

where we have assumed f to be continuous. We will heavily make use of the notion of fixed points.

The fixed point $\hat{x}$ is said to be *unstable* if

$$\{f^n(\hat{x} \pm \epsilon)\}_{n=0}^{\infty}, \quad \epsilon \in \mathbb{R} \tag{1}$$

diverges for all $\epsilon > 0$. It is said to be asymptotically or *locally stable* if we can find an $\epsilon > 0$ such that (1) converges and *stable* in the interval I if the sequence of iterates converges to $\hat{x}$ for all $x_0 \in I$.

It is possible to draw conclusions about the stability of the fixed point $\hat{x}$ of f by examining the slope within a small neighborhood of it (any open interval containing $\hat{x}$). The map f is locally stable at $\hat{x}$ if $|f'(\hat{x})| < 1$ and unstable if $|f'(\hat{x})| > 1$. We can see this by linearizing f about $\hat{x}$, i.e.

$$f(y_0) \approx \hat{x} + f'(\hat{x})(y_0 - \hat{x}),$$

which is an adequate approximation for y_0 sufficiently close to $\hat{x}$. Assuming

that $|f'(\hat{x})| < 1$, we have

$$\begin{aligned}|f(y_0) - \hat{x}| &= |\hat{x} + f'(\hat{x})(y_0 - \hat{x}) - \hat{x}| \\ &= |f'(\hat{x})(y_0 - \hat{x})| = |f'(\hat{x})||y_0 - \hat{x}| < |y_0 - \hat{x}|,\end{aligned}$$

so that $y_1 = f(y_0)$ is even closer to $\hat{x}$. By induction, it follows that

$$\lim_{n\to\infty} |f^n(y_0) - \hat{x}| = 0,$$

so that $\lim_{n\to\infty} y_n = \hat{x}$. Locally stable/unstable fixed points are also said to be *attractive/repellent*. The value $\lambda = f'(\hat{x})$ is also called the *multiplier* of f at $\hat{x}$. In addition, a fixed point $\hat{x}$ is said to be *superstable* if $f'(\hat{x}) = 0$ from which it immediately follows that $\hat{x}$ is also locally stable.

To show that there exists a unique stable fixed point to which all initial values in the interval I converge, we have to check that

$$|f(x) - f(y)| \leq a|x - y|, \quad \forall x, y \in I,\ a \in [0, 1). \tag{2}$$

Reshuffling the terms in the above definition, we can see that $|f'(x)|$ can take the role of a as $y \to x$. Compared to local stability, the difference here is that (2) has to be satisfied for all $x, y \in I$ so that we have global stability of some sort. A map that satisfies the above condition is called a *contraction mapping* for which a unique stable fixed point is guaranteed to exist. To see this, let $x_0 \in I$, $f(I) \subset I$, $m, n \in \mathbb{N}_0$ and $n < m$ where $\mathbb{N}_0$ denotes the set of natural numbers including 0. The set of non-zero natural numbers will be denoted by $\mathbb{N}_+$. We have

$$\begin{aligned}|x_n - x_m| &= |f(x_{n-1}) - f(x_{m-1})| = a|x_{n-1} - x_{m-1}| \\ &= a^2|x_{n-2} - x_{m-2}| = ... = a^n|x_0 - x_{m-n}| \\ &= a^n\left(|x_0 - x_1| + |x_1 - x_2| + ... + |x_{m-n-1} - x_{m-n}|\right) \\ &= a^n|x_0 - x_1|(1 + a + a^2 + ... + a^{m-n-1}) < \frac{a^n|x_0 - x_1|}{1 - a},\end{aligned}$$

where we have used the triangle inequality in the lines 3 & 4. The factor $1/(1-a)$ is the closed-form solution of the geometric series $\sum_{n=0}^{\infty} a^n$. Taking the limit, we obtain

$$\lim_{m,n\to\infty} |x_n - x_m| = \lim_{n\to\infty} \frac{a^n|x_0 - x_1|}{1 - a} = \lim_{n\to\infty} a^n M = 0,$$

as $a < 1$, so that the sequence is Cauchy whence $\hat{x} = \lim_{n\to\infty} x_n$ is convergent

within I provided that I is complete. The limit $\hat{x}$ is thus a fixed point. Uniqueness can be shown be noting that

$$|f(\hat{x}) - f(\hat{y})| = |\hat{x} - \hat{y}| \leq a|\hat{x} - \hat{y}| \implies |\hat{x} - \hat{y}| = 0 \implies \hat{x} = \hat{y},$$

having assumed $\hat{x}$ and $\hat{y}$ to be two distinct fixed points. The result is known as the Banach fixed-point theorem [5].

2.3 Orbits and periodic points

We now introduce another essential concept: that of orbits and periodic points. A point x is said to be periodic of period k if

$$f^k(x) = x \implies f^{nk}(x) = f^{(n-1)k}(x) = ... = x, \tag{3}$$

that is, if x is being revisited every k iterations by f. Intuitively, if the tail of a sequence of iterates oscillates periodically between k points, we talk about a k-orbit. The set of elements of a k-orbit is denoted by O^k and clearly $|O^k| = k$. All elements of O^k are thus periodic points of period k.

The definition of periodic points looks strikingly similar to that of a fixed point (cf. section 2.2). Indeed, all elements of O^k being period-k points are fixed points of f^k. To exemplify this, let the 2-orbit O^2 be given. Let $\hat{x}_1, \hat{x}_2 \in O^2$, $\hat{x}_1 \neq \hat{x}_2$, so that $f(\hat{x}_1) = \hat{x}_2$ and $f(\hat{x}_1) = \hat{x}_2$. We now have

$$f^2(\hat{x}_1) = f(f(\hat{x}_1)) = f(\hat{x}_2) = \hat{x}_1$$

and $f^2(\hat{x}_2) = \hat{x}_2$ by a similar argument. More generally, we can find the elements of O^k by looking at the solution set of $f^k(\hat{x}) = \hat{x}$. Fixed points are thus strictly speaking some kind of period-1 point or 1-orbit.

We now apply the concept of a fixed point's stability to orbits. The value $\lambda = \frac{d}{dx} f^k(\hat{x})$ is called the *multiplier* of the kth iterate of f at $\hat{x}$ (cf. section 2.2). By using the chain rule we can the see that

$$\begin{aligned}
\frac{d}{dx} f^k(\hat{x}) &= \frac{d}{dx}\left[f\left(f^{k-1}(\hat{x})\right)\right] = f'\left(f^{k-1}(\hat{x})\right) \cdot \left[\frac{d}{dx} f^{k-1}(\hat{x})\right] \\
&= f'\left(f^{k-1}(\hat{x})\right) \cdot f'\left(f^{k-2}(\hat{x})\right) \cdot \left[\frac{d}{dx} f^{k-2}(\hat{x})\right] \\
&= ... = \prod_{k=0}^{k-1} f'(f^k(\hat{x})) = \prod_{\hat{x} \in O^k} f'(\hat{x}),
\end{aligned} \tag{4}$$

where $f^0(\hat{x}) := \hat{x}$ and where we have used the fact that $O^k = \{f^k(\hat{x})\}_{n=0}^{k-1}$ for some $\hat{x} \in O^k$ in the last step. All elements of O^k being period-k points thus have the same multiplier which is the product of their derivatives of f. Analogous to the definition of locally stable and unstable fixed points, the k-orbit O^k is said to be locally stable if $|\lambda| = |\frac{d}{dx} f^k(\hat{x})| < 1$ and unstable if $|\lambda| > 1$.

Lastly, the k-orbit O^k is called *superstable* if it has multiplier $\lambda = 0$, i.e.

$$\lambda = \frac{d}{dx} f^k(\hat{x}) = 0, \quad \hat{x} \in O^k,$$

from which it follows by (4) that

$$\lambda = \prod_{\hat{x} \in O^k} f'(\hat{x}) = 0 \iff f'(\hat{x}) = 0, \tag{5}$$

for some $\hat{x} \in O^k$. That is, an orbit is superstable if and only if one of its elements is stationary.

2.4 Pitchfork bifurcation

Let $f_\mu(x) = f(\mu, x)$ be a map parametrized by μ. Most generally, the emergence of a qualitative change in the behavior of f_μ when varying the parameter μ is called a *bifurcation*. There exist many different kinds of bifurcations. The one that is pertinent to our discussion is characterized by the splitting of one fixed point into three fixed points when changing μ. Such a bifurcation is called *pitchfork bifurcation* as it resembles the three tines emerging from the shaft of a pitchfork. More precisely, this bifurcation is marked by a loss of stability of the fixed point $\hat{x}$ at the *bifurcation point* μ_0 whence two new stable fixed points emerge. The multiplier of $\hat{x}$ necessarily has absolute value equal to 1 at μ_0 as it it passing from local stability to instability (cf. section (2.2).

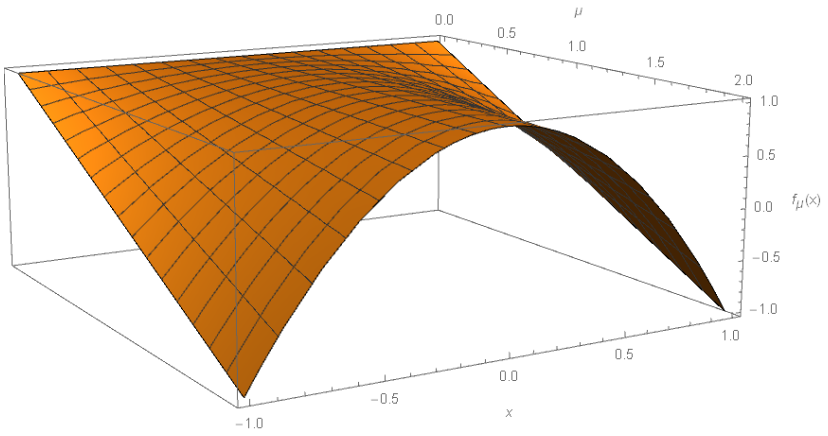

Figure 1: 3D plot of $f_\mu(x)$.

3 Basics

3.1 The one-hump map

In this paper we shall mainly be concerned with the following non-linear family of functions parametrized by μ (cf. fig. 1):

$$f_\mu(x) = 1 - \mu x^2, \quad x \in [-1, 1], \ \mu \in [0, 2].$$

This family is different from the well-known logistic map which was also used by Feigenbaum in his papers but is easier to work with while providing the same universal characteristics. One family can in fact be continuously transformed into the other by a combination of scaling and shifting. Observe that $f_\mu([-1, 1]) \subseteq [-1, 1]$, so that it is reasonable to consider the bounded sequence of iterates

$$\{x_n\}_{n=0}^{\infty} = \left\{f_\mu^n(x_0)\right\}_{n=0}^{\infty}, \quad x_0 \in [-1, 1].$$

3.2 Final-state diagram

By plotting the sequence of iterates of f_μ for different values of μ, we can observe very complex and partly chaotic behavior (cf. fig. 2). The interval $[0, \mu_\infty)$ in fig. 2 is marked by a series of successive *bifurcations* at μ_1, μ_2, etc. where the orbits' periods are repeatedly being doubled. The limit of the bifurcation points μ_n converges to μ_∞ as $n \to \infty$. We call μ_∞ the Feigenbaum point. The values λ_n mark the superstable points which will

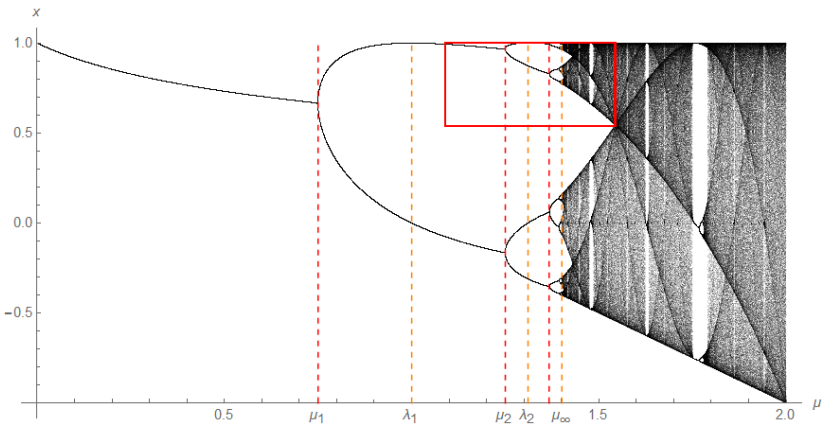

Figure 2: Final-state diagram of f_μ. The first 1900 out of 2000 iterates for each μ have been dropped for the orbit to emerge. From left to right we observe a cascade of period-doubling bifurcations at the points μ_n culminating in μ_∞. This is followed by very intricate and partly chaotic behavior. The region outlined by the red box resembles the entire diagram itself.

be talked about more thoroughly in section 3.4. For μ beyond μ_∞ we can see both chaotic regions with no apparent orbits and windows of stability in between exhibiting very regular behavior. At the end point $\mu = 2$, the iterates appear to be spread across all of $[-1, 1]$. We can also observe an intricate structure of bands beyond μ_∞ where the points seem to cluster more densely.

Perhaps the most remarkable property is the diagram's *self-similarity* which is illustrated by the red box in fig. 2. Magnifying the diagram so as to show only the contents of this box, we obtain a picture that is qualitatively the same as the original diagram, i.e. it has the same of properties described earlier although the scales might differ somewhat. The process of magnifying a section to obtain a self-similar copy can naturally be repeated infinitely many times where infinitely many other points of fig. 2 can serve as focal point. We will later see that the scaling necessary to produce these self-similar copies gives rise to two universal constants.

To illustrate Feigenbaum scaling, we will primarily focus on the interval $[0, \mu_\infty)$ as it provides all of the necessary characteristics. The entire discussion, by virtue of self-similarity, could have been based on any other one of

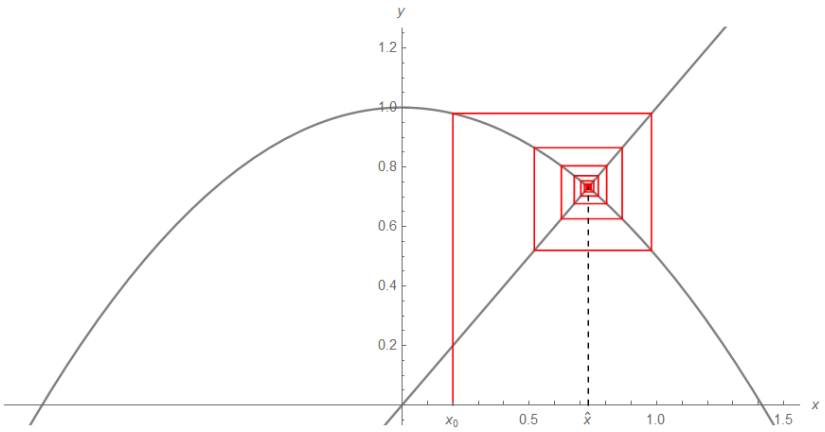

Figure 3: Cobweb plot of the first 100 iterates of $f_\mu(x)$ for $\mu = 0.5 < \mu_1$, $x_0 = 0.2$, $|f'_{0.5}(\hat{x})| \approx 0.73 < 1$. The fixed point is attractive.

an infinitude of non-empty subwindows.

3.3 Bifurcation Cascade

For $\mu \in [0, \mu_1) = [0, 0.75)$ the sequence of iterates converges to $\hat{x}$ so that $\hat{x}$ is a fixed point of f_μ (cf. section 2.2). This is exemplified in the cobweb plot (fig. 3) for $\mu = 0.5$ which is a useful way of visualizing iterations. Solving $f_\mu(\hat{x}) = \hat{x}$ for $\hat{x}$, we obtain

$$\hat{x} = \frac{\sqrt{4\mu + 1} - 1}{2\mu},$$

where $\lim_{\mu \to 0} \hat{x}_\mu = 1$ and requiring that $\hat{x} \in [-1, 1]$.

Examining the derivative of f at $\hat{x}$, we have

$$\left| f'_\mu(\hat{x}) \right| = \left| 1 - \sqrt{4\mu + 1} \right| < 1 \quad \text{for } \mu \in [0, \mu_1),$$

so that $\hat{x}$ is locally stable for these parameter values (cf. section 2.2).

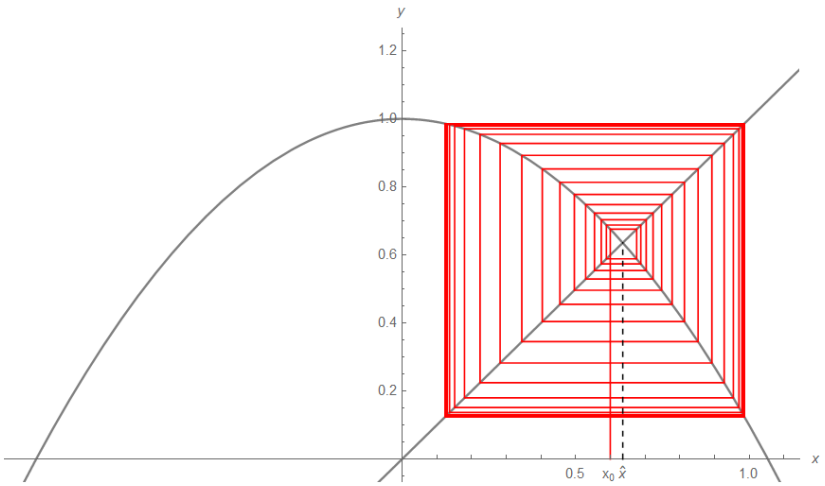

Figure 4: $f_\mu(x)$ for $\mu = 0.9 > \mu_1$, $x_0 = 0.6$, $|f'_{0.9}(\hat{x})| \approx 1.14 > 1$. The fixed point is repellent as the slope of f_μ at $\hat{x}$ has absolute value greater than 1.

Furthermore,

$$\begin{aligned} & |f_\mu(x) - f_\mu(y)| \leq a|x - y| \\ \implies & \mu|y^2 - x^2| = \mu|y - x||y + x| \leq a|x - y| \\ \implies & \mu|x + y| \leq a \implies 2\mu \leq a \implies \mu \in [0, 0.5) \end{aligned}$$

for $x, y \in [-1, 1]$, $a \in [0, 1)$, so that f_μ is a contraction mapping for such μ-values whence all sequences of iterates are guaranteed to converge to $\hat{x}$ by the Banach fixed-point theorem (cf. section 2.2). For $\mu \in [0.5, 0.75)$, f fails to be a contraction so that other techniques are required to prove global stability.

At μ_1, we observe the first pitchfork bifurcation (cf. section 2.4). For $\mu > \mu_1$ we have $|f_\mu(\hat{x})| > 1$, so that $\hat{x}$ is now the unstable middle tine of the pitchfork. For $\mu \in [\mu_1, \mu_2)$, the tail of the sequence of iterates now oscillates between two values (cf. fig. 4), i.e. a stable 2-orbit is born. These two points are now fixed points of f^2 (cf. section 2.2). Observe that $\hat{x}$ is a fixed point of f^2 as well as

$$f_\mu^2(\hat{x}) = f_\mu(f_\mu(\hat{x})) = f_\mu(\hat{x}) = \hat{x},$$

although it is now unstable. Since $\hat{x}$ is repellent, the probability of choosing

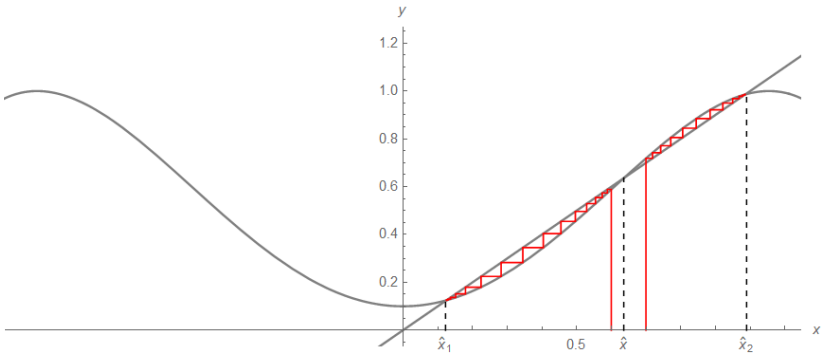

Figure 5: $f_\mu^2(x)$ for $\mu = 0.9 > \mu_1$ with the initial values $[x_0, y_0] = [0.6, 0.7]$. The fixed point $\hat{x}$ is repellent while $\hat{x}_1$ and $\hat{x}_2$ are attractive.

exactly that value out of uncountably many $x \in [-1, 1]$ is effectively zero. That is the reason for its absence in the final-state diagram for $\mu > \mu_1$.

At $\mu_2 = 1.25$, the two fixed points of f^2 lose stability in turn whence we obtain a stable 4-orbit by the same principle. We then get an 8-orbit at μ_3 and so on ad infinitum. We denote by μ_n the parameter value at which the previously stable 2^{n-1}-orbit is becoming unstable i.e. where the nth pitchfork bifurcation into a stable 2^n-orbit happens. The elements of O^{2^n} are now stable fixed points of f^{2^n}.

We could go about determining the orbits' elements for higher periods by analytically solving the fixed-point equations $f^{2^n}(x) = x$ but this would be increasingly difficult as the degree of f^{2^n} grows at a doubly exponential rate, i.e. $deg(f^{2^n}) = 2^{2^n}$

3.4 Feigenbaum universality

We now introduce the first of the two universal constants and the class of maps for which they are valid. The distance between successive bifurcation points is nearly geometric, that is

$$\delta = \lim_{n\to\infty} \frac{d_n}{d_{n+1}} = 4.669201... \quad \text{for } d_n = \mu_{n+1} - \mu_n. \tag{6}$$

The limit δ is called the *Feigenbaum constant* after its discoverer and it is exactly the same for any one family of maps out of our class of one-hump maps. We define it here more rigorously which is mainly for the purpose of

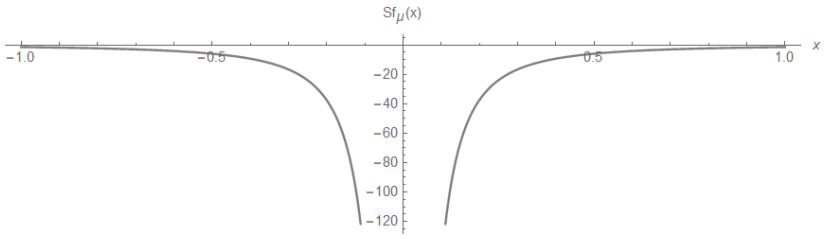

Figure 6: The Schwarzian derivative $Sf_\mu(x)$ for any $0 < \mu \leq 2$.

reference. We have [4]:

Table 1: Universality Conditions

(i) $f : [a, b] \to [a, b]$ is smooth.
(ii) f has exactly one *quadratic* maximum at x_{max} in (a, b), i.e. $f''(x_{max}) \neq 0$.
(iii) f is strictly increasing in $[a, x_{max})$ and strictly decreasing in $(x_{max}, b]$.
(iv) f has negative Schwarzian derivative (cf. fig. 6), i.e.

$$Sf(x) = \frac{f'''(x)}{f'(x)} - \frac{3}{2}\left(\frac{f''(x)}{f'(x)}\right)^2 < 0 \; \forall x \in [a, b].$$

Note that such maps need not be symmetrical about the vertical line going through their maximum point (cf. $\mu x^2 \sin(\pi x)$). Examples of other such maps are given by

$$\begin{aligned} &\mu x(1-x), \quad \mu \in [0, 4], \quad x \in [0, 1], \quad \mu_\infty \approx 3.569945 \\ &\mu \sin \pi x, \quad \mu \in [0, 1], \quad x \in [0, 1], \quad \mu_\infty \approx 0.865579, \end{aligned} \tag{7}$$

where the first one is known as the logistic map.

The limit to which the bifurcation points μ_n converge is called the *Feigenbaum point* and it is *not* universal as exemplified in (7). For our map $f_\mu(x) = 1 - \mu x^2$, we have

$$\mu_\infty = \lim_{n\to\infty} \mu_n = 1.401155....$$

There will be a more detailed discussion about the behavior of the iterates of f_μ at this point in section 5.1.

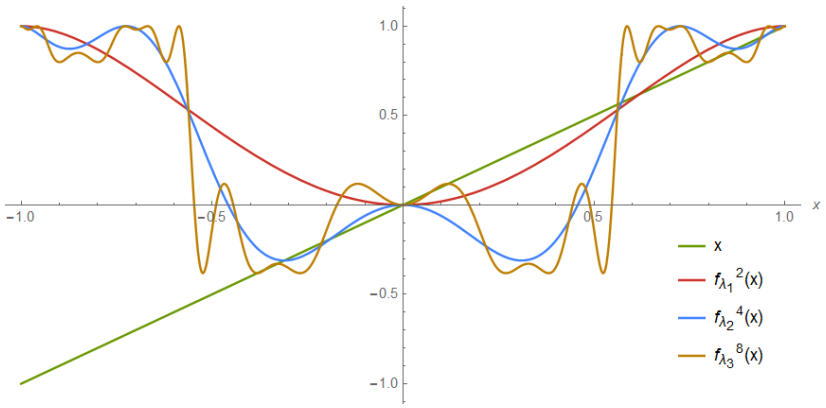

Figure 7: Several superstable iterates of f_μ. Observe that they are all stationary at the fixed point $x = 0$.

Recall that an orbit O^k is said to be superstable if $\frac{d}{dx} f^k(\hat{x}) = 0$ for all $\hat{x} \in O^k$ which is equivalent to $f'(\hat{x}) = 0$ for some $\hat{x} \in O^k$ (cf. section 2.3). This is in turn equivalent to $0 \in O^k$ for f_μ as its only stationary point is at $x = 0$ provided that $\mu > 0$ (cf. fig. 7). We denote the parameter values for which there exists a superstable 2^n-orbit by λ_n, where n is any positive natural number (cf. table 3 in section 6.1). The slope at the fixed points of $f_\mu^{2^n}$ for $\mu < \mu_\infty$ during which they are stable ranges from 1 to -1 for increasing μ so that the λ_n can be found midway between μ_n and μ_{n+1} (cf. fig. 2). It is possible to modify the definition of the Feigenbaum constant and point by replacing the bifurcation points with the superstable points, i.e.

$$\delta = \lim_{n\to\infty} \frac{\Delta_n}{\Delta_{n+1}} \quad \text{for } \Delta_n = \lambda_n - \lambda_{n+1} \text{ and } \mu_\infty = \lim_{n\to\infty} \lambda_n. \tag{8}$$

It is easier to calculate the Feigenbaum constants by employing the superstable points which will be seen in section 6.1.

The second universal constant is the scaling factor α whose name will become apparent later. It is intimately related to δ in that it is the limit of the ratio between a superstable orbit's smallest non-zero element and the other such element of the next higher superstable orbit (cf. fig. 8). That is

$$\alpha = \lim_{n\to\infty} \frac{\Lambda_n}{\Lambda_{n+1}} = -2.502907... \quad \text{for } \Lambda_n = \min_{\hat{x}\in O^{2^n}_{\lambda_n}\setminus\{0\}} |\hat{x}|. \tag{9}$$

Analogous to δ being the limit of the ratios of the horizontal distances Δ_n

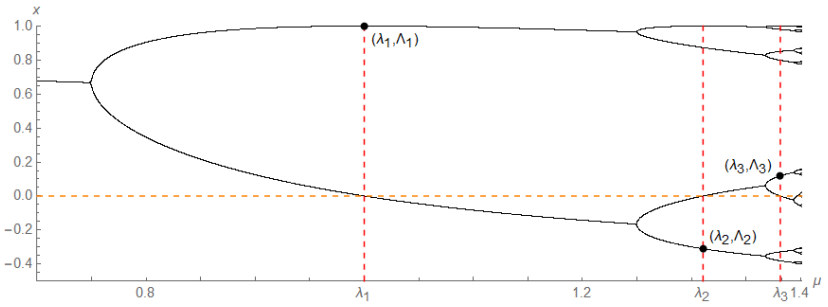

Figure 8: Superstable orbits in the bifurcation diagram. Observe that the line $x = 0$ crosses the bifurcation graph at every superstable parameter value. The constants δ and α are approximated by the ratios of distances of the μ and x-coordinates of (λ_n, Λ_n) respectively (cf. (8) & (9)). The smallest non-zero elements of the superstable orbits oscillate between positive and negative x-values as α is negative.

(cf. (8)) in the final-state diagram (fig. 2), α is instead the limit of the vertical distances Λ_n (cf. fig. 8). The two universal constants δ and α are also called *Feigenvalues* collectively.

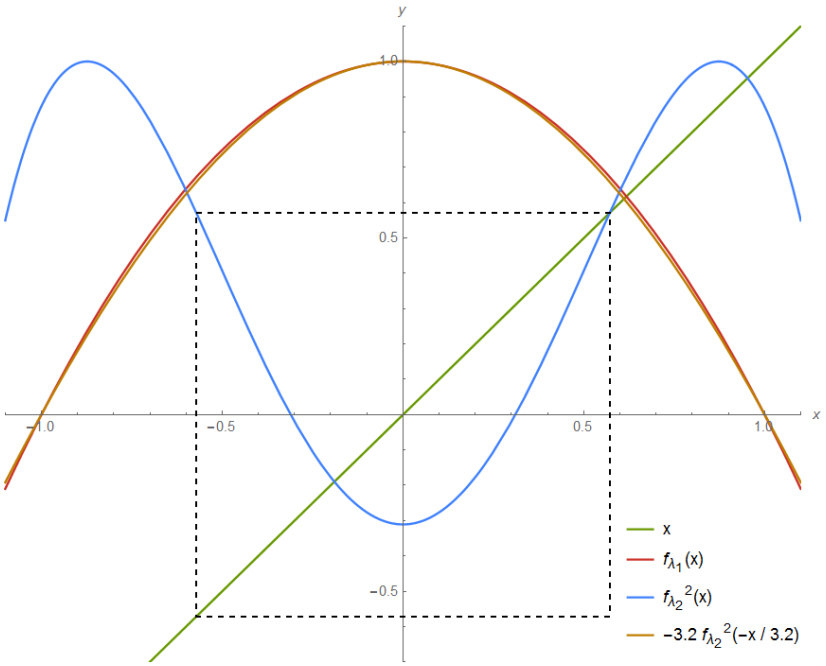

Figure 9: The graph of f^2 within the dashed box can be transformed so as to resemble f. Note that the transformed graph of f^2 will not be exactly the same as f. Here it is quartic instead of quadratic. The scaling factor is approximately 3.2 in this case but converges quickly to α when performing the same transformation for higher iterates. Note the different superstable parameter values that were taken.

4 Renormalization

4.1 The period-doubling transformation

In fig. 9 we can see that the graph of f^2 can be made to look similar to f by a combination of reflection and magnification. The same procedure can be performed for higher iterates as well where the factor by which we magnify f^2 converges to α as will be seen later. The process of obtaining a function similar to f from higher iterates is called *renormalization*. We can define this similarity transformation $F : \mathfrak{F} \to \mathfrak{F}$ by

$$F(h)(x) = \alpha h^2(x/\alpha), \quad h \in \mathfrak{F}, \tag{10}$$

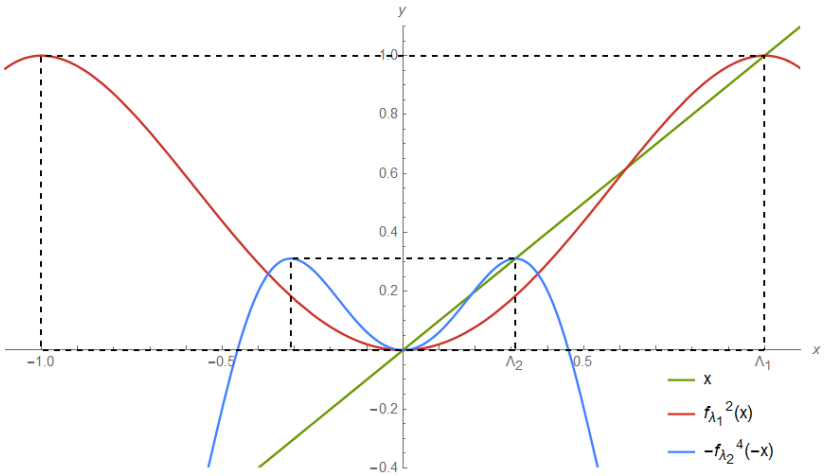

Figure 10: Visualization of the scaling factor α. Note that $f^4_{\lambda_2}(x)$ has already been reflected about both axes to emphasize the similarity to $f^2_{\lambda_1}(x)$. The values Λ_1 and Λ_2 denotes the smallest non-zero elements of the superstable orbits of period 2 and 4 respectively. The points even closer to the origin where the line $y = x$ and the graph of f^n intersect are unstable fixed points so that they are not part of these orbits.

which we call *period-doubling transformation* henceforth. $\mathfrak{F}$ denotes the Banach space (complete normed vector space) of bounded smooth functions equipped with the supremum norm. When being passed a function h, this operator reflects $h \circ h$ about both axes and magnifies it by the constant factor α. Given f^{2^n}, we can apply the above transformation n times to obtain a function resembling f.

In fig. 10, we can observe that the factor by which we need to scale is the ratio between a superstable orbit's smallest non-zero element and the other such element of the next higher superstable orbit. This is exactly the definition of the universal constant α whence it was called scaling factor.

We shall later see that F has a unique fixed point g normalized by requiring that $g(0) = 1$. This fixed point is rather a fixed function as F is operating in function space. We also call g the universal function as it is the fixed point universal to our class of one-hump maps (cf. table 1). It also holds information about the two Feigenvalues δ and α. The stability of the fixed point

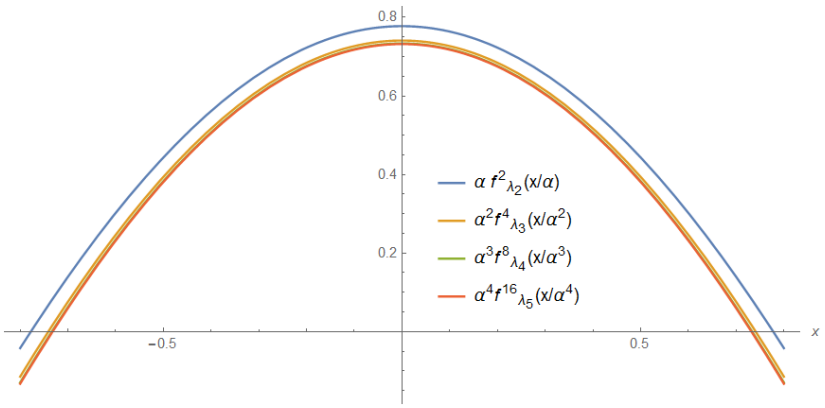

Figure 11: g_1 is converging rapidly with the rate of pointwise convergence approaching δ.

g depends on the direction from which it is being approached in function space.

We now construct a sequence of functions that converges to g. The rate of convergence of this sequence will also be of major importance. Let

$$g_1(x) = \lim_{n\to\infty} \alpha^n f^{2^n}_{\lambda_{n+1}}(x/\alpha^n),$$

which is the limit of successive renormalizations of f_{λ_1}. This limit is convergent as is visualized in fig. 11.

More generally, define g_r as the limit of successively renormalizing f_μ at its rth superstable parameter, i.e.

$$g_r(x) = \lim_{n\to\infty} \alpha^n f^{2^n}_{\lambda_{n+r}}(x/\alpha^n), \tag{11}$$

which is convergent [1] for all $r \in \mathbb{N}_0$ (cf. fig. 12).

Now let

$$g(x) = \lim_{r\to\infty} g_r(x) = \lim_{n\to\infty} \alpha^n f^{2^n}_{\lambda_\infty}(x/\alpha^n), \tag{12}$$

where $\lambda_\infty = \mu_\infty$ is the Feigenbaum point. We will now show that g is a *fixed point* of F (10), i.e. that g is invariant under this transformation.

By definition

$$\begin{aligned} F(g_r) &= \lim_{n\to\infty} \alpha^{n+1} f_{\lambda_{n+r}}^{2^{n+1}}(x/\alpha^{n+1}) \\ &= \lim_{k\to\infty} \alpha^{k} f_{\lambda_{k+(r-1)}}^{2^{k}}(x/\alpha^{k}) = g_{r-1}, \end{aligned} \tag{13}$$

where $k = n+1$, so that F lowers the index of g_r by 1. From this it follows that

$$F(g) = F\left(\lim_{r\to\infty} g_r\right) = \lim_{r\to\infty} F(g_r) = \lim_{r\to\infty} g_{r-1} = g \tag{14}$$

as F is continuous (cf. fig. 12). The fixed function g is furthermore *unstable* along the line $\{g_r\}$ in function space parametrized by r. One can see this by introducing a small perturbation $\tilde{g}$ of g perturbed in the direction along the line $\{g_r\}$. Such a perturbation can be found by choosing g_{r_ϵ} for very large r_ϵ. The repeated application of F to then moves $\tilde{g} = g_{r_\epsilon}$ farther away from g (cf. (14)).

Observe also that F (cf. (10)) is scale invariant i.e. $-\beta g(-x/\beta)$ is also a fixed point of F for some non-zero constant β [3]. This can easily be verified numerically once g has been found. We make g the unique fixed point by requiring that $g(0) = 1$. Plugging into (10) we obtain

$$\begin{aligned} F(g) = g \implies \alpha g(g(0)) = g(0) \\ \iff \alpha g(1) = 1 \iff \alpha = \frac{1}{g(1)}, \end{aligned} \tag{15}$$

so that α is in fact dependent on g.

4.2 The linearized period-doubling transformation

As indicated in the previous section, the rate of convergence of g_r to g is the same as that for μ_n and λ_n (cf. (6) & (8)), i.e.

$$\lim_{r\to\infty} \frac{g_r(x) - g_{r+1}(x)}{g_{r+1}(x) - g_{r+2}(x)} = \delta, \quad \forall x \in [-1, 1],$$

which was confirmed numerically. Recall that g was unstable under F along $\{g_r\}$ (cf. (14)), so that the *rate of divergence* in that direction is δ, which is thus an *eigenvalue* of the *derivative* dF_g of F at g (cf. fig. 12). This is one of the key concepts of this thesis and opens up another path for computing δ. It leads us to one of Feigenbaum's conjectures stating that δ is the largest eigenvalue of dF_g [1]. In section 6.2 we will find the eigenvalues of dF_g

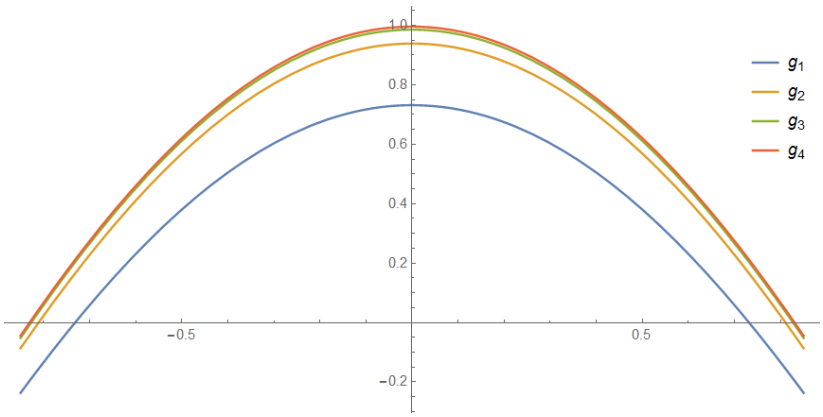

Figure 12: g_r converges pointwise to g with rate δ as $r \to \infty$. The plot approximates the g_r using $n = 7$ (cf. (11)) which provides a very close estimate.

numerically to validate this fact.

Differentiating F at g, we are taking the Gateaux derivative. This is a generalization of the ordinary derivative where we now deal with a limit of functions in function space instead of ordinary finite-dimensional vectors. We compute

$$\begin{aligned} dF_g(h) &= \lim_{\tau \to 0} \frac{F(g+\tau h) - F(g)}{\tau} = \frac{d}{d\tau} F(g+\tau h)\Big|_{\tau=0} \\ &= \frac{d}{d\tau}\left[\alpha\left[g+\tau h\right]^2\left(\frac{x}{\alpha}\right)\right]\Big|_{\tau=0} \\ &= \alpha \frac{d}{d\tau}\left[g\left(g\left(\frac{x}{\alpha}\right)+\tau h\left(\frac{x}{\alpha}\right)\right)+\tau h\left(g\left(\frac{x}{\alpha}\right)+\tau h\left(\frac{x}{\alpha}\right)\right)\right]\Big|_{\tau=0} \\ &= \alpha\left[g'\left(g\left(\frac{x}{\alpha}\right)\right) h\left(\frac{x}{\alpha}\right) + h\left(g\left(\frac{x}{\alpha}\right)\right)\right], \quad g, h \in \mathfrak{F} \end{aligned}$$

while making use of the chain rule in the last step and assuming α to be constant [8].

Analogous to the multiplier of fixed points (cf. section 2.2), the magnitude of an eigenvalue gives clue about the transformation's stability in the associated direction. We can illustrate this by introducing a small perturbation to the

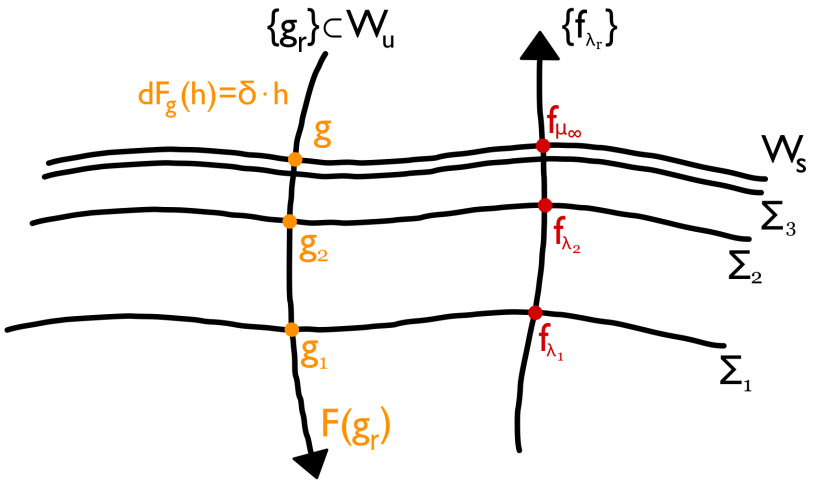

Figure 13: Schematic diagram in function space showing the fixed function g along with the lines $\{g_r\}$ and $\{f_{\lambda_r}\}$. W_u and W_s denote the unstable and stable manifold respectively. F is expanding along W_u and contracting along W_s. If we perturb g in the direction associated with δ then the repeated application of F moves the perturbation farther away from g (cf. (13) & (16)). Similarly, applying F repeatedly to f_{μ_∞}, we can observe convergence to g, as it lies on W_s. Σ_n denote the surfaces of one-hump maps which are superstable with period 2^n.

fixed function g, i.e. let

$$g_\epsilon = g + \epsilon h, \quad h \in \mathfrak{F}.$$

Now by linearizing F about g, we have for ϵ sufficiently small that

$$F(g_\epsilon) = F(g + \epsilon h) \approx F(g) + \epsilon dF_g(h) = g + \epsilon \lambda h,$$

where λ denotes an eigenvalue of dF_g. Applying F repeatedly to g_ϵ we obtain

$$F^n(g_\epsilon) = g + \epsilon \lambda^n h. \tag{16}$$

Letting n tend to infinity, we observe that F is stable in directions where $|\lambda| < 1$ and unstable where $|\lambda| > 1$ [10]. The subspace of the infinite-dimensional vector space $\mathfrak{F}$ where F is stable/unstable is called the stable/unstable manifold respectively. The line $\{g_r\}$ corresponding to the eigenvalue δ is thus part of the unstable manifold. Another eigenvalue is α which will be verified numerically in section 6.2. Similar to the terminology of repellent and attractive fixed points (cf. section 2.2), F is said to be expanding along the unstable manifold and contracting on the stable manifold (cf. fig. 13).

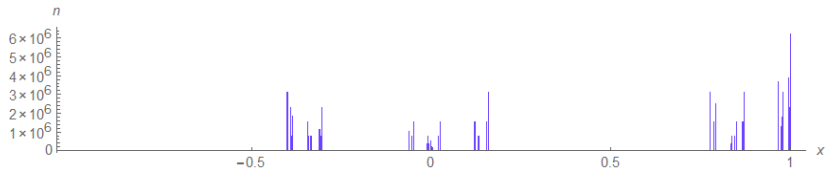

Figure 14: Histogram plot of the first 10^8 iterates of f_{μ_∞} divided into 1000 bins, $x_0 = 0.5$, μ_∞ was approximated by an estimate of λ_{15}. We can observe many gaps and tight clustering. The plot is in fact an approximation of the Cantor set which is self-similar.

5 At and beyond the Feigenbaum point

5.1 At the Feigenbaum point

At μ_∞ the iterates of f_μ converge to an orbit with infinitely many elements which we denote by O_{μ_∞}. In fact,

$$|O_{\mu_\infty}| = \lim_{n\to\infty} |O_{\mu_n}| = \lim_{n\to\infty} 2^{n-1} = \lim_{k\to\infty} 2^k,$$

so that O_{μ_∞} is uncountable (there exists no injection from it to the set of natural numbers). The distribution of the orbit's elements across $[-1, 1]$ is visualized in fig. 14. Every point of O_{μ_∞} seems to have other points lying nearby. Due to the self-similar nature of the histogram, this still holds true when zooming in arbitrarily far. Thus for any $x \in O_{\mu_\infty}$ and every interval $I_x = (x - \epsilon, x + \epsilon)$, I_x contains some elements of O_{μ_∞} other than x itself. A point x for which this is true is called a *limit point* so that all elements of O_{μ_∞} are limit points [12].

There are also gaps of different sizes in fig. 14 where no points lie at all. Thus we can again argue by self-similarity that for any $x \in O_{\mu_\infty}$ and every interval $I_x = (x - \epsilon, x + \epsilon)$, there are gaps in I_x i.e. points in I_x that are not contained in O_{μ_∞}. A point $x \in X$ for which this is true is said not to belong to the *interior* of X so that O_{μ_∞} has empty interior.

The set O_{μ_∞} can in fact be constructed in a similar way to the *Cantor ternary set*, which results from removing the open set comprising the middle third of the original interval and doing the same for the resulting two subintervals ad infinitum. The final set is then the intersection of all such subintervals. To construct O_{μ_∞} in this way we need to remove open sets of variable sizes with the rest of the procedure being the same [4]. The complement of O_{μ_∞}

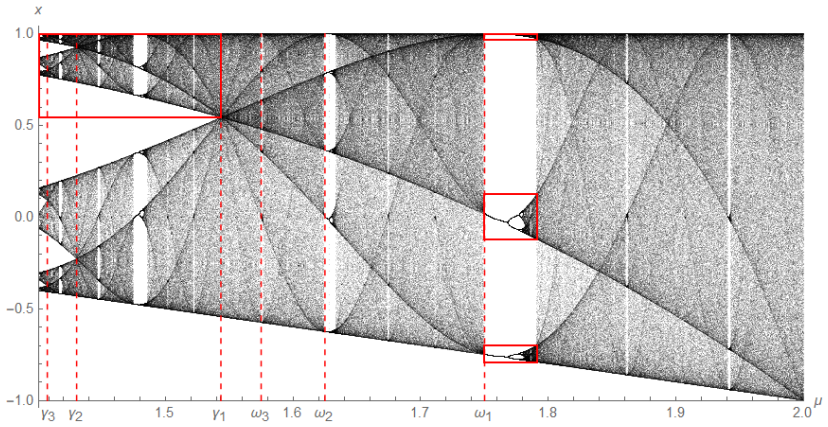

Figure 15: Final-state diagram of f_μ for $\mu \geq \mu_\infty$. The red window in the upper-left corner is similar to the diagram itself with the other three windows to the right being similar to the entire final-state diagram (fig. 2). The parameters γ_n and ω_n mark the nth reverse bifurcation point and the onset of a stable $(2n+1)$-orbit respectively.

consists then of a union of open sets so that O_{μ_∞} is closed (by De Morgan's laws).

A closed set whose elements are all limit points is also called a *perfect set* and a closed set that has empty interior is called *nowhere dense*. Cantor sets in general and O_{μ_∞} in particular are both perfect and nowhere dense sets.

5.2 Beyond the Feigenbaum point

In fig. 15 we can see that the distribution of the iterates at γ_1 looks like two distorted copies of the case where $\mu = 2$. The part of the diagram where $\mu \leq \gamma_1$ consists in fact of two regions that are self-similar to all of fig. 15 (up to reflecting and stretching) where the upper region is outlined with a red box. We can define γ_1 to be at the same μ-value as the right border of this self-similarity window. This self-similarity naturally repeats itself infinitely many times so that we can keep zooming into this window. Once the magnified portion of fig. 15 looks similar to the original, there will be another such self-similarity window at the same position. We can thus define γ_n to be at the same width as the right border of the nth of these nested windows. Having based their definition on self-similarity, it may not

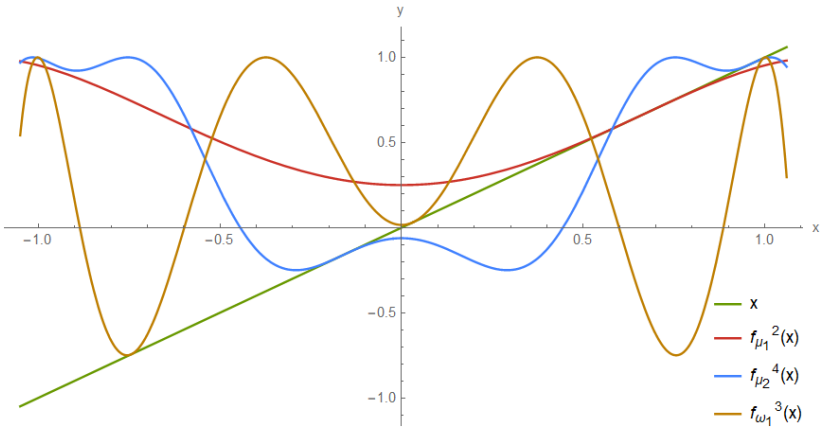

Figure 16: f_μ^n for $n = 2, 3, 4$ at their respective bifurcation points. The slope of the graphs at the previously stable fixed points is exactly 1 as they are about to bifurcate.

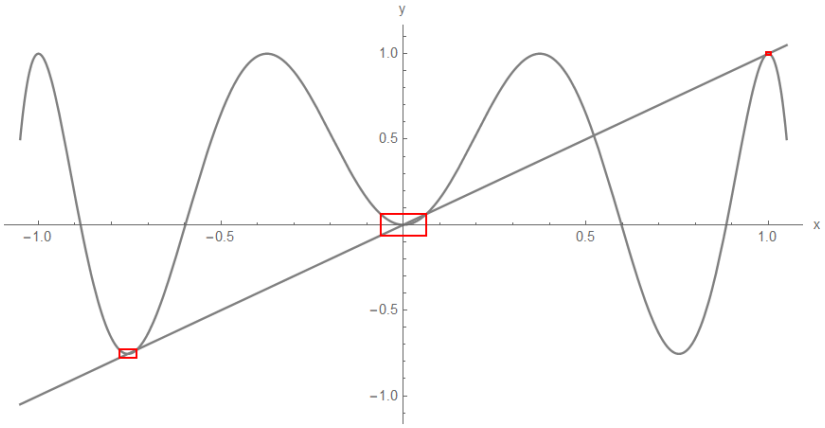

Figure 17: f_μ^3 at $\mu \approx 1.7549$ where it is superstable. The three self-similar regions of f^3 are outlined with red boxes with the rightmost box barely visible (cf. $f_{\lambda_1}^2$ in fig. 10).

be very surprising that

$$\lim_{n\to\infty} \frac{\gamma_n - \gamma_{n+1}}{\gamma_{n+1} - \gamma_{n+2}} = \delta,$$

as the scaling factor in parameter space necessary to produce self-similar copies is δ. We call those values *reverse bifurcation points* as they are approaching μ_∞ in the same fashion as the bifurcation points μ_n but this time from the right instead of from the left.

There are many regions of stable periodic orbits between the chaotic regions of fig. 15, the most salient of which is the period-3 window beginning at $\mu = \omega_1 = 1.75$. The process by which this stable orbit emerges from where there has previously been chaos is called *tangent bifurcation*. Indeed, ω_1 is exactly the parameter value for which the third iterate of f is tangential to the line $y = x$ (cf. fig. 16). Recall from section 3.3 that a fixed point bifurcation is marked by the loss of stability of the previously stable fixed points with twice as many new stable fixed points emerging. In fact, given any non-empty open interval $I_\mu \subset [0, 2]$, we can find stable periodic orbits for some $\mu \in I_\mu$ [4].

Fig. 17 shows the superstable case of f_μ^3 where the three red boxes enclose regions that are similar to f_μ^2 at its superstable point λ_1 (cf. fig. 10). Increasing the parameter slightly we can observe a cascade of successive pitchfork bifurcations for each one of the three regions which yields orbits of the periods $3 \cdot 2^n$. Further to the left of fig. 15 at ω_2 a 5-orbit is born in the same fashion which then results in orbits of the periods $5 \cdot 2^n$ when raising the parameter value. There are in fact stable n-orbits for every positive natural number n. The ordering in which they appear gives rise to the so called Sharkovsky sequence (cf. table 2) where finding an orbit of period n for some system of iterated transformations implies that there are also orbits of period k with k occurring after n in that sequence [4]. The ordering is as follows:

Table 2: The Sharkovsky sequence

$3, 5, 7, 9, 11, ...$	$\{2^0(2k+1),\ k \in \mathbb{N}_+\}$
$2 \cdot 3, 2 \cdot 5, 2 \cdot 7, 2 \cdot 9, 2 \cdot 11, ...$	$\{2^1(2k+1),\ k \in \mathbb{N}_+\}$
...	
$2^n \cdot 3, 2^n \cdot 5, 2^n \cdot 7, 2^n \cdot 9, 2^n \cdot 11, ...$	$\{2^n(2k+1),\ k \in \mathbb{N}_+\}$
...	
$..., 2^5, 2^4, 2^3, 2^2, 2, 1$	$\{2^k,\ k \in \mathbb{N}_0\}$

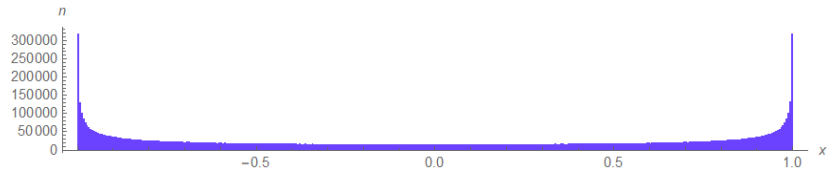

Figure 18: Histogram plot of the first 10^7 iterates of f_μ at $\mu = 2$ divided into 500 bins, $x_0 = 0.2$.

The existence of a 3-orbit thus implies that there exist orbits of all other possible periods.

5.3 At the end point

At $\mu = 2$, the sequence of iterates behaves *chaotically* which means there is a great *sensitivity* to initial conditions i.e. small perturbations in the initial value become amplified arbitrarily. Given any non-empty open interval $I \subset [-1, 1]$, the points of I will eventually be spread across all of $[-1, 1]$. This property is called *mixing* and is another characteristic of chaos [4]. It follows naturally from sensitivity in our case as $[-1, 1]$ is bounded. Any non-empty open subset I necessarily contains uncountably many points which are then separated from each other when iterated however close they were initially. The non-uniform shape of the distribution shown in fig. 18 can be explained by the non-linearity of f_μ which tends to squeeze the values further to the boundary points. In addition, the sequence of iterates is dense in $[-1, 1]$ for most initial values i.e. any non-empty open interval $I \subset [-1, 1]$ contains some points of $\{f^n(x_0)\}$ for some fixed x_0 (cf. O_{μ_∞} in section 5.1). This does not mean that there are no initial values for which $\{f_2^n(x_0)\}$ results in an orbit. In fact, there exist such values in every non-empty open interval $I \subset [-1, 1]$ so that the set of initial values that yield an orbit is dense in $[-1, 1]$. The existence of *dense periodic orbits* is another necessary condition for chaos [4]. Note that all of these orbits are unstable.

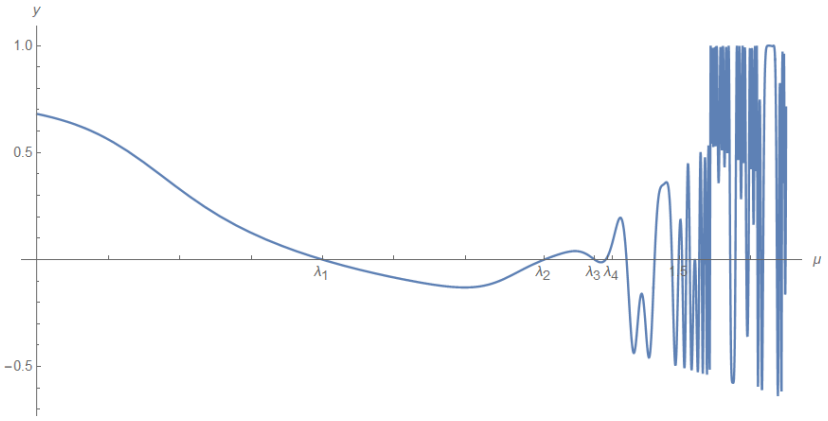

Figure 19: The graph of $f_\mu^{2^4}(0)$. There are numerous roots beyond μ_∞ as the degree of $f_\mu^{2^n}(0)$ increases at a doubly exponential rate i.e. $deg(f_\mu^{2^n}(0)) = 2^{(2^n-1)} - 1$. This makes root-finding by brute force impractical for high iterates despite being only interested in the roots below μ_∞.

6 Computational Part

6.1 Computing the Feigenvalues directly

It is possible to compute δ and α directly by making use of the superstable points. We know from (5) that superstable orbits contain the point where f achieves its maximum. Thus solving the fixed-point equation

$$f_\mu^{2^n}(x_{max}) = x_{max} \implies f_\mu^{2^n}(0) = 0 \tag{17}$$

for μ, we have converted the original problem into a root-finding problem (cf. fig. 19). The solution set of (17) consists of all parameter values for which we have a superstable orbit of period 2^n or a factor thereof. Recall that fixed points of certain iterates of f remain fixed points of higher iterates although they lose their stability.

In order to find the roots, we will make use of Newton's method which converges quadratically for initial values sufficiently close to the root in question. Plugging (17) into the iterative scheme, we obtain

$$r_{k+1} = r_k - \frac{h(r_k)}{h'(r_k)} = r_k - \frac{f_{r_k}^{2^n}(0)}{\frac{d}{d\mu} f_{r_k}^{2^n}(0)}, \quad r_0 \in [0, 2].$$

The derivative can be calculated iteratively as well by

$$\begin{aligned}\frac{d}{d\mu}f_\mu^{2^n}(x) &= \frac{d}{d\mu}\left[f_\mu^{2^{(n-1)}}\left(f_\mu^{2^{(n-1)}}(x)\right)\right] \\ &= \tfrac{d}{d\mu}\left[f_\mu^{2^{(n-1)}}\right]\left(f_\mu^{2^{(n-1)}}(x)\right)\cdot\tfrac{d}{d\mu}\left[f_\mu^{2^{(n-1)}}(x)\right],\end{aligned}$$

where we have made use of the chain rule.

Having computed $\lambda_{n-2}, \lambda_{n-1}$, and λ_n we can find an estimate of the next superstable point by

$$\lambda_{n+1} = \lambda_n + \frac{\lambda_n - \lambda_{n-1}}{\delta_n},$$

where

$$\delta_n = \frac{\lambda_{n-1} - \lambda_{n-2}}{\lambda_n - \lambda_{n-1}}$$

is the $(n-2)$th estimate of δ. To obtain an initial estimate of δ, we can determine the first three superstable points analytically by using Mathematica's `Solve[]` function [14]. Table 3 lists the results up to the 12th superstable point.

We can now approximate the universal function g and the scaling factor α by equations (12) and (9) respectively or determine α from g by (15). The precision of all these values is very limited by the increasing computational cost of evaluating high iterates of f however.

Table 3: The first 12 superstable points together with estimates of δ.

n	λ_n	δ_n
1	1	
2	1.31070264	
3	1.38154748	4.385678
4	1.39694536	4.600949
5	1.40025308	4.655130
6	1.40096196	4.666112
7	1.40111380	4.668549
8	1.40114633	4.669061
9	1.40115329	4.669172
10	1.40115478	4.669195
11	1.40115510	4.669200
12	1.40115517	4.669201

6.2 Finding the spectrum of dF

It is feasible to determine the fixed function g by employing a collocation method [3, 2, 8, 9]. That is, we evaluate the period-doubling fixed-point equation at a finite number of points $\{x_i\}_1^n$ which represent a function, thus reducing an infinite-dimensional problem to a finite-dimensional one. We represent f by a truncated Chebyshev series [8, 9], i.e.

$$f(x) \approx \tilde{f}(x) = \sum_{i=0}^{n} c_i T_i(x), \tag{18}$$

where the c_i are the coefficients and T_n Chebyshev polynomials of the first kind. These polynomials are intimately related to the trigonometric functions used in Fourier series as well as being mutually orthogonal with respect to a certain inner product. They can be defined recursively by

$$\begin{aligned} T_0(x) &= 1, \\ T_1(x) &= x, \\ T_{n+1}(x) &= 2xT_n(x) - T_{n-1}(x). \end{aligned}$$

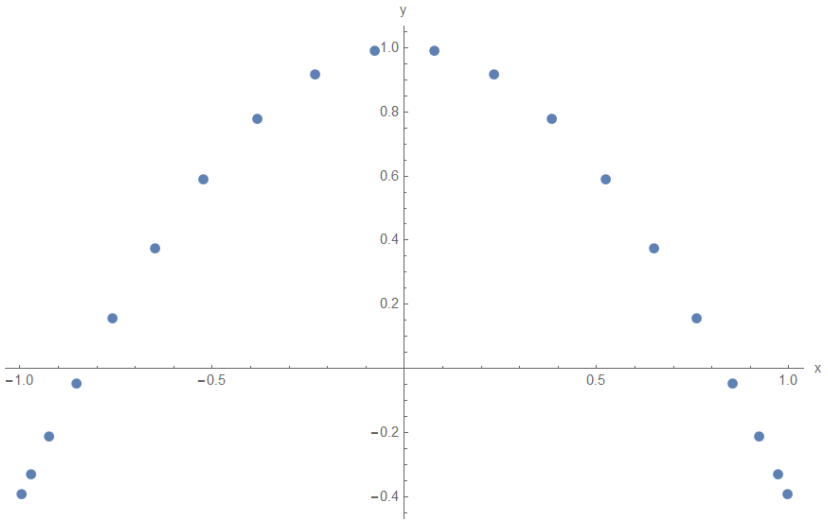

Figure 20: A close approximation of the fixed function g at the Chebyshev nodes $\{x_i\}$ obtained after 5 Newton–Raphson iterations.

The function f is evaluated at the n points called Chebyshev nodes (cf. fig. 20) given by

$$x_i = \cos\left(\frac{(2i-1)\pi}{2n}\right), \quad i = 1, ..., n. \tag{19}$$

The choice of interpolation points is not crucial. The Chebyshev nodes mitigate the problem of Runge's phenomenon i.e. heavy oscillation near the boundary points of the interval in question when interpolating. However, equispaced interpolation points work as well [2].

The period-doubling fixed-point equation (cf. (10) & (15)) is defined by

$$\Phi(g) = g - F(g) = g(x) - g^2(g(1)\,x)/g(1) = 0. \tag{20}$$

Evaluating (20) at the nodes (19), we obtain a system of n equations in n variables:

$$\Phi(g_1, ..., g_n) = \Phi(\tilde{g}) = \begin{bmatrix} g_1 - \tilde{g}^2(\tilde{g}(1)\,x_1)/\tilde{g}(1) \\ \vdots \\ g_n - \tilde{g}^2(\tilde{g}(1)\,x_n)/\tilde{g}(1) \end{bmatrix} = \begin{bmatrix} 0 \\ \vdots \\ 0 \end{bmatrix}, \quad g_i = \tilde{g}(x_i), \tag{21}$$

where $\tilde{g}$ is inferred from the g_i by making use of the discrete Chebyshev transform (cf. (18)). The coefficients are determined as follows:

$$\begin{aligned} c_0 &= \frac{1}{n}\sum_{i=0}^{n-1} g_i, \\ c_j &= \frac{2}{n}\sum_{i=0}^{n-1} g_i T_j(x_i), \quad j = 1, ..., n. \end{aligned} \tag{22}$$

We again use Newton–Raphson iterations for solving (21), but this time in n dimensions. We have

$$\tilde{g}_{j+1} = \tilde{g}_j - d\Phi_j^{-1} \cdot \Phi(\tilde{g}_j),$$

where $\tilde{g}_j$ denotes the jth approximation of $\tilde{g}$ and $d\Phi_j^{-1}$ the inverted Jacobian matrix of $\Phi(\tilde{g}_j)$ approximated by finite differences, i.e.

$$d\Phi = \begin{bmatrix} \Delta_1\Phi & \dots & \Delta_n\Phi \end{bmatrix} \approx \begin{bmatrix} \frac{\partial\Phi_1}{\partial g_1} & \cdots & \frac{\partial\Phi_1}{\partial g_n} \\ \vdots & \ddots & \vdots \\ \frac{\partial\Phi_n}{\partial g_1} & \cdots & \frac{\partial\Phi_n}{\partial g_n} \end{bmatrix},$$

where

$$\Delta_i\Phi = \frac{\Phi(g_1, ..., g_i + \epsilon, ..., g_n) - \Phi(\tilde{g})}{\epsilon}.$$

The initial values $\tilde{g}_0 = \{f_{1.4}(x_i)\}$ were chosen and $\epsilon = 10^{-7}$ proved to be a good perturbation size. The number of nodes was fixed to $n = 20$ and the convergence to the fixed function was quadratic, the difference after only 5 iterations compared to the previous one being less than $6 \cdot 10^{-15}$ under the supremum norm. Fig. 20 shows $\tilde{g}$ after the final iteration. The scaling factor α can now simply be determined by $\alpha = 1/\tilde{g}(1)$ (cf. (15)).

We now proceed to finding δ as well as other eigenvalues of the linearized period-doubling transformation. Recall that

$$dF_g(h) = \alpha\left[g'\left(g\left(\frac{x}{\alpha}\right)\right) h\left(\frac{x}{\alpha}\right) + h\left(g\left(\frac{x}{\alpha}\right)\right)\right], \tag{23}$$

assuming that α is constant [8]. We can now define a linear operator $M : \mathbb{R}^n \to \mathbb{R}^n$ by

$$M(h_1, ..., h_n) = M(\tilde{h}) = dF_g(\tilde{h})(x_1, ..., x_n),$$

where $\tilde{h}$ is inferred again from the discrete Chebyshev transform (22).

The eigenvalue of the largest magnitude can now be determined by the power method. That is, we consider the normalized sequence of iterates $\{M^n b/||M^n b||_2\}$ for some non-zero initial vector b where $||\cdot||_2$ denotes the Euclidean norm. This sequence converges to the eigenvector associated with the eigenvalue of the largest magnitude which we call the most dominant eigenvalue henceforth. Intuitively, the effect of a linear finite-rank operator M acting on vector b can be expressed as a linear combination of its eigenvectors whose coefficients involve the corresponding eigenvalues. This can be done by changing the basis to be the set of all eigenvectors of M provided that they span the whole space. The repeated application of M to b is thus most pronounced in the direction associated with the most dominant eigenvalue so that the other directions become increasingly neglected. Once the most dominant eigenvector v_1 has been found it is easy to find its associated eigenvalue by $(M[v_1], v_1)/(v_1, v_1)$, where $(\cdot, \cdot)$ denotes the dot product. In order to find the second-most dominant eigenvalue, we can now remove the contribution of v_1 from the sequence of iterates by projecting them onto the subspace spanned by the remaining eigenvectors. This leads us to Arnoldi's method [9]. It relies on the information provided by the space of the first m iterates $\{M^n b\}_{n=0}^{m-1}$ which is called a Krylov subspace [11]. This space is then successively orthogonalized through a form of Gram-Schmidt process whence the most dominant eigenvectors emerge in decreasing order.

Both methods are very suitable as they don't require M to be explicitly defined as a matrix. The 10 most dominant eigenvalues together with their analytic expression are listed in the table below.

Table 4: The first 10 eigenvalues of dF_g.

n	ζ_n	
1	4.669201	δ
2	-2.502907	α
3	1	
4	-0.399535	α^{-1}
5	0.159628	α^{-2}
6	-0.123652	
7	-0.063777	α^{-3}
8	-0.057307	
9	0.025481	α^{-4}
10	-0.010180	α^{-5}

Recall that we assumed the scaling factor α to be constant in (23). It is however dependent on g (cf. (15)), so that it need not be constant in a neighborhood of g. Differentiating F at g without that assumption we obtain a different linearization dF' whose spectrum contains α^2 as the largest eigenvalue [8]. The constant δ remains an eigenvalue of dF' in this case although now being smaller than α^2. This would violate Feigenbaum's conjecture of δ being the largest eigenvalue and the unstable manifold would have one more dimension as a result.

6.3 Generalized Feigenvalues

We can generalize f as follows to allow for non-quadratic maxima [2]:

$$f_{\mu,d}(x) = 1 - \mu|x|^d, \quad d \in (1, 12].$$

For $d \neq 2$, these families of maps are not part of our class of one-hump maps as they violate universality condition (ii) (cf. table 1). There exists nonetheless some kind of universality with the generalized Feigenvalues depending on the choice of d (cf. fig. 21). We furthermore have that $\delta_d \to 2$ as $d \to 1$ [6].

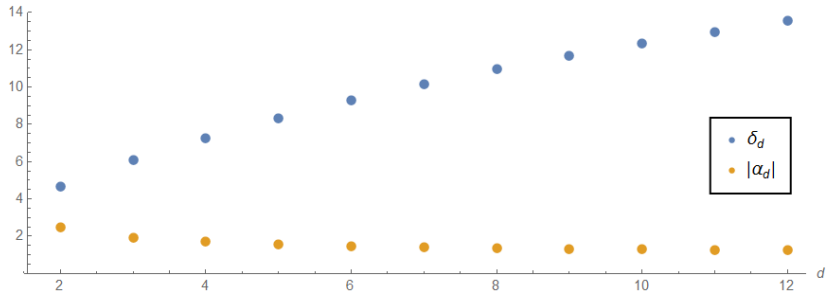

Figure 21: Feigenbaum constant and scaling factor of $f_{\mu,d}(x)$ for different values of d.

7 Conclusion

Feigenbaum scaling turned out to be a rather broad topic with plenty to explore, drawing from disciplines like functional analysis, chaos theory, topology, numerical analysis, statistical mechanics and fractal geometry. Its study can aid in the understanding of chaotic systems, when they arise and how to recognize them. Not a lot of additional research has been conducted in the last couple of decades with the first proofs of Feigenbaum's conjectures being presented in the 80s [6, 13]. The most recent papers mentioned in this work were primarily concerned with the spectrum of the linearized period-doubling transformation (23) and how to compute it [8, 9]. I tried to adapt on open attitude toward Feigenbaum's conjectures, stating them only in their most general terms, as there seems to be some disagreement as to the dimensionality of the unstable manifold [8]. By the *Feigenbaum conjecture* is usually meant that δ is the only eigenvalue of dF_g (23) outside the unit disk [2, 10, 6]. This only seems to be true if α is assumed to be constant when deriving dF_g and the space operated on is restricted to even functions–the fixed function g is even after all. There exist, however, non-even functions satisfying the universality conditions (cf. table 1) so that this seems unnecessarily restrictive [8]. Finally, I hope I have succeeded in shedding some light on the subject matter as well as having stirred some interest for further reading and exploration.

References

[1] Mitchel J. Feigenbaum, Quantitative Universality for a Class of Nonlinear Transformations, Journal of Statistical Physics, Vol. 19, 1978

[2] Keith Briggs, Feigenbaum Scaling in Discrete Dynamical Systems, Doctoral thesis, University of Melbourne, 2001

[3] Mitchel J. Feigenbaum, "Universal Behavior in Nonlinear Systems", Physica 7D (1983) p. 16-39 North-Holland Publishing Company, Reprinted with minor additions and with permission from Los Alamos Science, Vol. I, No. 1, p. 4-27, 1980

[4] Heinz-Otto Peitgen, Hartmut Jürgens, Dietmar Saupe, Chaos and Fractals: New Frontiers of Science, Second Edition, Springer, 2004

[5] A. N. Kolmogorov, S. V. Fomin, Introductory Real Analysis, Revised English Edition, Dover Publications, 1970

[6] Pierre Collet, Jean-Pierre Eckmann, Iterated Maps on the Interval as Dynamical Systems, Reprint of the 1980 Edition, Birkhäuser

[7] Robert M. May, Simple Mathematical Models With Very Complicated Dynamics, Nature Vol. 261, June 10 1976

[8] V.P. Varin, Spectral Properties of the Period-Doubling Operator, Keldysh Institute preprints, 2011, 009, 20 pp.

[9] Andrea Molteni, An efficient method for the computation of the Feigenbaum constants to high precision, 2016, `https://arxiv.org/pdf/1602.02357.pdf`

[10] A.J. Lichtenberg, M.A. Lieberman, Regular and Chaotic Dynamics, Second Edition, Springer, 1992

[11] Yousef Saad, Numerical Methods for Large Eigenvalue Problems, Second edition, 2011, Society for Industrial and Applied Mathematics

[12] James Munkres, Topology, Second Edition, Pearson New International Edition, Pearson, 2013

[13] Oscar E. Lanford, A computer-assisted proof of the Feigenbaum conjectures. Bull. Amer. Math. Soc. (N.S.) 6 (1982), no. 3, 427–434

[14] Janek Sendrowski, Mathematica code supplementary to this thesis, 2020, `https://github.com/Sendrowski/Feigenbaum-Scaling`